Journal Pre-proof

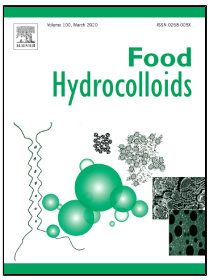

Tannic acid-assisted cross-linked nanoparticles as a delivery system of eugenol: The characterization, thermal degradation and antioxidant properties.

Dandan Cao, Chengsheng Jia, Suping Ji, Xiaoming Zhang, Bertrand Muhoza

PII:	S0268-005X(19)31801-6
DOI:	https://doi.org/10.1016/j.foodhyd.2020.105717
Reference:	FOOHYD 105717
To appear in:	*Food Hydrocolloids*
Received Date:	08 August 2019
Accepted Date:	26 January 2020

Please cite this article as: Dandan Cao, Chengsheng Jia, Suping Ji, Xiaoming Zhang, Bertrand Muhoza, Tannic acid-assisted cross-linked nanoparticles as a delivery system of eugenol: The characterization, thermal degradation and antioxidant properties., *Food Hydrocolloids* (2020), https://doi.org/10.1016/j.foodhyd.2020.105717

Graphical Abstract

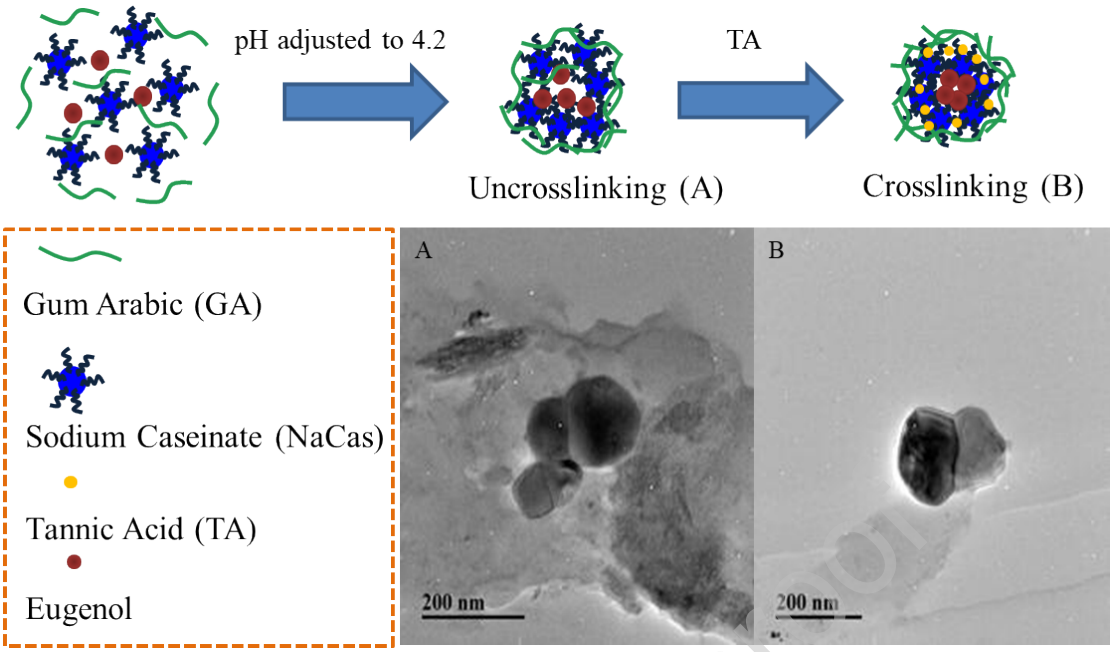

Tannic acid-assisted cross-linked nanoparticles as a delivery system of eugenol: The characterization, thermal degradation and antioxidant properties.

Dandan Cao, Chengsheng Jia,* Suping Ji, Xiaoming Zhang, and Bertrand Muhoza

State Key Laboratory of Food Science and Technology, School of Food Science and Technology, Jiangnan University, 1800 Lihu Road, Wuxi 214122, Jiangsu, China

* To whom correspondence should be address. E-mail: chshjia@126.com.

Abstract: In this paper, eugenol-loaded nanoparticles (sodium caseinate and gum arabic) cross-linked by tannic acid were prepared and characterized. The fourier transform infrared spectroscopy, fluorescence spectrum and circular dichroism confirmed the reaction mechanism between eugenol or tannic acid and protein. Circular dichroism demonstrated that the addition of tannic acid had a great impact on the secondary structure of sodium caseinate. The encapsulation efficiency of eugenol reached 70% and the particle size was about 150 nm. Thermal gravimetric analysis revealed that the degradation temperature of eugenol significantly increased from 77-230 °C to 200-387 °C through the nanoencapsulation. Additionally, the nanoparticles cross-linked by tannic acid remained stable at acidic conditions and after 15 days of storage, and also exhibited slow release and improved antioxidant effects. Therefore, this study provided new insights into the interaction mechanism between polyphenols and proteins, and the possibility of nano-delivering plant essential oils and bioactive molecules using tannic acid as the crosslinking agent.

Keywords: eugenol; cross-linking; sodium caseinate; tannic acid; nanoparticles

1. Introduction

Eugenol (4-ally-2-methoxyphenol, $C_{10}H_{12}O_2$), as the main active ingredient of clove essential oil, is natural phenolic compound extracted from clove. It is widely used to improve storage stability due to its spectral bacteriostatic and antioxidant properties (Šibul, et al., 2016). However, most plant essential oils are sensitive to heat, highly volatile and water insoluble, which limits their application (Woranuch & Yoksan, 2013). Recently, various delivery systems have been designed to improve the stability, solubility and control-release ability of essential oils, such as emulsion (Zhang, Pan, & Zhong, 2017), biopolymer nanoparticles (Woranuch, et al., 2013), solid lipid nanoparticles (Cortial, Vocanson, Valour, Urbaniak, & Briançon, 2014), liposomes (Liolios, Gortzi, Lalas, Tsaknis, & Chinou, 2009) and microcapsules (Sharif, et al., 2017). Compared to microencapsulation, nanoencapsulation has recently become an interesting technique due to the benefits of stability improvement, retention of volatile ingredients, controlled-release ability, and water solubility improvement of hydrophobic ingredients (Woranuch, et al., 2013). Among these delivery systems, biopolymer nanoparticles obtained by complex coacervation have several favorable properties including easy design and preparation, biocompatibility, structure variations and interesting biomimetic characters, attracting the interest of many researchers (Faridi Esfanjani & Jafari, 2016; Hudson & Margaritis, 2014).

Recently, proteins and polysaccharides are the major raw materials for the preparation of biopolymer nanoparticles obtained by complex coacervation due to their biodegradability, biocompatibility, low toxicity and abundance. Sodium

caseinate (NaCas) is a commercially available and water soluble protein component produced by the acid precipitation of casein micelles from milk, which has excellent surface activity, stability and self-assembling properties, and is a good material for the preparation of nanocarriers (Pereira, 2014). Meanwhile, gum arabic (GA) is also an ideal carrier material, has good water solubility and emulsification stability, and is biocompatible, non-toxic and biodegradable.

However, studies have reported that the stability of nanoparticles obtained by complex coacervation is not good under certain conditions including pH, ionic strength. Therefore, the cross-linking strategies have been used to stabilize the protein-based nanoparticles and improve their delivery potentials. Chemical cross-linkers (such as glutaraldehyde) could crosslink protein and polysaccharides to improve the stability of nanoparticles under different environmental conditions (Chang, Wang, Hu, & Luo, 2017). However, the chemical cross-linkers are toxic and therefore cannot meet requirements for green-label. In addition, some enzymes (such as transglutaminase, laccases) have been also used to be cross-linkers, however, have strict requirements for pH, substrate, and temperature. In addition, the high cost can also limit the application of enzymes. Contrary to enzymes, polyphenols (the plant secondary metabolite) have aromatic rings and OH groups, which are highly reactive to proteins and amino acids (Muhoza, Xia, & Zhang, 2019). Furthermore, several previous studies demonstrated that polyphenols can interact with proteins over a wide range of pH (Thongkaew, Gibis, Hinrichs, & Weiss, 2014). Recently, some studies also demonstrated that polyphenols could interact with proteins, carbohydrates and

lipids based on different non-covalent bonds including hydrogen bonds, hydrophobic interactions and the others, and also interact through covalent bonds (Kroll, Rawel, & Rohn, 2003).

Tannic acid (TA), a kind of polyphenol rich in hydroxyl groups, can interact strongly with polysaccharides and proteins (Xie, Wehling, Ciftci, & Zhang, 2017), and has many beneficial properties such as antioxidant, antibacterial, and antiviral properties (Zou, Guo, Yin, Wang, & Yang, 2015). Zou, et al. (2015) reported that zein nanoparticles cross-linked by TA showed better resistance to digestion, and the insoluble protein complexes further strengthened the network of nanoparticles. It has been reported that the stability of emulsion formed by ovalbumin-TA was improved by the increased electrostatic repulsions (Chen, et al., 2018). The main forces between protein and TA include hydrogen bonding, electrostatic interactions and hydrophobic interactions. In addition, the covalent bond may also form between TA and protein under extreme conditions (Xie, et al., 2017). Although many studies have been conducted to crosslink-proteins using TA, few reports have investigated on TA crosslinked nanoparticles prepared by NaCas and GA coacervates for the delivery of eugenol.

The aim of this study was to prepare and characterize eugenol-loaded nanoparticles cross-linked by TA, and was to explore the feasibility of using TA as a cross-linker to crosslink protein nanoparticles. The interaction mechanisms of eugenol and TA with NaCas were investigated by means of circular dichroism (CD), fourier transform infrared spectroscopy (FTIR) and fluorescence spectroscopy. The thermal

83 gravimetric analysis (TGA) was used to study thermal degradation properties of
84 nanoparticles. Moreover, the encapsulation efficiency (EE), morphology, particle
85 characteristic and of uncrosslinked and crosslinked nanoparticles were also reported.
86 The delivery potential of nanoparticles was systematically studied, including
87 antioxidant capacity, storage stability, slow release and controlled-release properties
88 under the simulated gastrointestinal conditions.

89

90 **2. Materials and methods**

91 ***2.1 Materials***

92 NaCas (moisture content 10.0 ± 0.9%) was from Shanghai Macklin Biochemical
93 Co., Ltd. GA was (moisture content 7.2 ± 0.4%) purchased from Sinopharm Chemical
94 Reagent Co., Ltd. Eugenol (purity about 96%) was from Ji'an Zhong Xiang natural
95 plant Co., Ltd. TA (AR, moisture content ≤12.0%) was purchased from Sinopharm
96 Chemical Reagent Co., Ltd. Glucono-δ-lactone (GDL) was bought from Henan three
97 chemical Biotechnology Co., Ltd. All other chemicals are chemical analytical level.

98 ***2.2. Preparation of eugenol-loaded nanoparticles***

99 The nanoparticles were prepared according to the method descripted by Ye,
100 Flanagan, and Singh (2006) with a slight modification. NaCas (10 mg/mL, w/v) and
101 GA (10 mg/mL, w/v) were dissolved in deionized water, respectively, stirred for at
102 least 3 h, and hydrated overnight at 4 ^{o}C as the stock solution for experiment. The
103 eugenol ethanol solution (3%, w/v) was added dropwise to the NaCas solution
104 according to certain core-wall ratios (0:1, 1:4, 1:3, 1:2, 1:1 and 2:1, w/w),

magnetically stirred for 30 min, and then the polysaccharide solution was added dropwise (NaCas/GA, 1:2, w/w) maintaining the total polymer concentration of 3 mg/mL. After stirring for 30 min, the mixture solution was adjusted to pH 4.2 using GDL solution (10%, w/v). After complex coacervation, the TA solution (10%, w/v) was added into the complex nanoparticles according to the different concentrations (0, 0.05%, 0.1%, 0.2%, 0.3% and 0.4%, w/v), adjusted the pH 4.2, and magnetically stirred for 3 h at room temperature to promote the formation of nanoparticles.

2.3. Measurements of particle size, particle size distribution and zeta-potential

Particle size, particle size distribution and zeta-potential were determined based on the principle of dynamic light scattering with multi-angle particle size and high sensitivity zeta potential analyzer (Nano Brook Omni， Brookhaven Instrument Corporation, America). The scattering angle was selected as backscattering mode with an angle of 173 °. The zeta-potential measurement was conducted using the same instrument with an electrode. The samples were diluted to the appropriate concentration for all experiments.

2.4. Encapsulation efficiency (EE)

EE is an indispensable indicator for evaluating the quality of nanoparticles. The solvent extraction method depicted by Muhoza, et al. (2019) was the most commonly used method to measure EE. The sample was dissolved in ethanol and ultrasonically assisted for 1 h to promote complete dissolution of eugenol for determination of total oil content. After ultrasonic extraction, the sample was centrifuged at 4300 × g for 30 min, and the supernatant was diluted to obtain permeate for HPLC (Zhang, et al.,

127 2017). The HPLC analysis was performed using a 1200 series HPLC system (Waters
128 1525 Binary HPLC Pump, Waters, Shanghai, China) with a SunFire C_{18} column (5
129 μm; 150 mm by 4.6 mm Column; Waters, Shanghai, China). The detector wavelength
130 was 282 nm. The injection volume of samples was 10 μL. A binary solvent mixture of
131 water (containing 0.1% formic acid) and acetonitrile was used at a linear gradient
132 from 25% to 75% acetonitrile within 20 min for elution. The flow rate was 0.6
133 mL/min, and the column temperature was controlled at 35 ºC. A standard curve was
134 prepared using the standard solution of eugenol dissolved at 50–200 μg/mL in
135 ethanol. The surface oil content was measured by dissolving samples in hexane.
136 Finally, the concentration of eugenol was determined using the standard curve
137 measured above (y=34235x+156002, R^2=0.9983). The EE was estimated according to
138 the following equation.

139 $$EE(\%) = (1 - \frac{Surface\ oil\ content}{Total\ oil\ content}) \times 100 \quad (1)$$

140 ***2.5. Fourier transform infrared spectroscopy (FTIR) analysis***

141 The spectra of all samples were conducted using the KBr tablet method on a
142 fourier transform infrared spectrometer (Nicolet IS10, Thermo Nicolet Corporation,
143 America) with a wavelength range of 400-4000 cm^{-1}, the resolution of 4 cm^{-1} and 32
144 scans.

145 ***2.6. Fluorescence spectroscopy***

146 Fluorescence spectroscopy (F-7000, Hitachi, Japan) was used to study the
147 interaction between eugenol or TA and NaCas. The eugenol nanoparticle solution
148 with different core wall ratios was diluted to the appropriate concentration. The

fluorescence spectroscopy was conducted at excitation wavelength of 280 nm or 295 nm. The emission spectra were obtained from 290 to 550 nm, both the slit width of excitation and emission width were 5 nm, the scanning voltage was 550 V, and the scanning speed was 1200 nm/min. The data recorded at the maximum fluorescence were used to calculate the binding constant (K_b) and binding sites (n) by the double-logarithm equation for static quenching (Velmurugan, Singam, Jonnalagadda, & Subramanian, 2014).

$$\frac{F0}{F} = e^{((K_{sv}[Q]))} = e^{((K_q T_0[Q]))} \quad (2)$$

$$log_{10}\frac{(F_0 - F)}{F} = log_{10}K_b + nlog_{10}[TA] \quad (3)$$

Where F_0 and F are the fluorescence intensities in the absence and presence of TA, respectively, and [TA] is the concentration of TA. K_{sv}, K_q and T_0 are the quenching constant, the bimolecular quenching rate constant and the lifetime of fluorescence in the absence of a quencher (10^{-8}), respectively (Zhang, et al., 2008). The K_b and n values are the association constant and the association site, respectively.

2.7. Circular dichroism (CD) analysis

The CD analysis was conducted using a chirascan V100 spectropolarimeter (Chirascan V100, Applied Photophysics Ltd, England), and the CD spectra were collected in a range of 180-260 nm with a 1nm bandwidth. The temperature was 25 ^{o}C. The sample solutions were diluted appropriately before measuring the CD spectra. The obtained data was processed properly to acquire the content of the secondary structure of protein.

2.8. Morphological observation

171 The morphologies of uncrosslinked and crosslinked nanoparticles were analyzed
172 by transmission electron microscopy (TEM) (JEM-2100, JEOL, Japan). The
173 acceleration voltage was 80 kV. For TEM measurement, a drop of the freshly
174 prepared dispersion was added to a carbon-coated copper grid (200 mesh) and then
175 observed using TEM. After drying, the carbon-coated copper grid loaded with the
176 nanoparticles was negatively stained with 2% phosphotungstic acid solution for 30
177 min. Then, the excess stain was removed using filter paper. Some photographs of
178 nanoparticles were taken using TEM.

179 ***2.9. Thermal gravimetric analysis (TGA)***

180 The thermal degradation properties of the samples were analyzed using a thermo
181 gravimetric analyzer (TGA2, METTLER TOLEDO Instrument, Switzerland), with
182 the temperature range of 30-600 ^{o}C, heating rate of 20 ^{o}C/min and nitrogen flow rate
183 of 20 mL/min. The thermos-gravimetric curves of the samples were measured
184 separately. Their derivative thermos-gravimetric (DTG) curves were also obtained
185 after processing.

186 ***2.10. pH and thermal stability of nanoparticles***

187 The pH and thermal stability were determined by the following procedure. The
188 sample solution was diluted to obtain a total polymer concentration of 1 mg/mL. The
189 diluted solution was adjusted to pH 3.0, 4.0, 5.0, 6.0 and 7.0 to study the pH stability
190 of the nanoparticles. The diluted solution was heated at 60, 80, 90 and 100 ^{o}C to study
191 the thermal stability of the nanoparticles according to the previous method (Joye,
192 Davidov-Pardo, & McClements, 2015).

2.11. Antioxidant capacity of nanoparticles

2.11.1. DPPH free radical scavenging capacity

DPPH free radical scavenging capacity of free eugenol and encapsulated eugenol nanoparticles was determined by making certain modification to the method of Wang, et al. (2016). Eugenol ethanol solution (3 mg/mL, w/v) was prepared, which was diluted into different concentration gradients using ethanol. Meanwhile, the prepared eugenol nanoparticle solution was diluted into different concentration gradients containing the same amount of eugenol with free eugenol. Two milliliters of sample were mixed with 2 mL DPPH ethanol solution and placed in the dark for 30 min after vortex to measure the absorbance value at wavelength of 517 nm. The solution containing 2 mL deionized water and 2 mL ethanol was used as a blank. The formula for calculating DPPH free radical scavenging rate was as follows.

$$\text{DPPH free radical scavenging rate (\%)} = \left(1 - \frac{A_s - A_c}{A_0}\right) \times 100 \quad (4)$$

Where A_0 and A_s are the absorption of DPPH solution added with deionized water and sample solution, respectively. A_c is the absorption of 4 mL deionized water added with sample solution.

2.11.2. $ABTS^+$ free radical scavenging capacity

$ABTS^+$ free radical scavenging capacity of free eugenol and eugenol-loaded nanoparticles (uncrosslinked and crosslinked) were determined by the method depicted previously (Shi, Yang, Zhang, & Yu, 2012). The sample solution (0.1 mL) diluted to different concentration gradients was added to 3.8 mL of $ABTS^+$ working solution, thoroughly mixed by vortex, and cultivated in the dark for 6 min. The

absorbance was measured at 734 nm. The scavenging rate of $ABTS^+$ free radical was calculated according to the following formula.

$$ABTS^+ \text{ free radical scavenging rate } (\%) = (1 - \frac{A_1}{A_0}) \times 100 \quad (5)$$

Where A_0 is the absorbance value of 0.1 mL ethanol (or pH 4.2 of distilled water) and 3.8 mL of $ABTS^+$ working solution. A_1 is the absorbance value of 0.1 mL sample solution and 3.8 mL of $ABTS^+$ working solution.

2.11.3. Total reducing power

The total reducing power of all the samples was measured using a previous method with several modifications (Zhu, et al., 2018). Briefly, 0.6 mL of phosphate buffer (0.2 mol/L) and 1.5 mL of $K_3Fe(CN)_6$ (1%, w/v) were added into the sample solution (1 mL) diluted to appropriate concentration gradients. The mixture was shook evenly and incubated at 50 °C water bath for 20 min. After cooling to room temperature, 2.5 mL of trichloroacetic acid (10%, w/v) were added the resultant solutions. After standing for 10 min, the solutions were centrifuged at 3000 × g for 10 min. Hereafter, 3 mL of supernatant was mixed with 0.2 mL of $FeCl_3$ (1%, w/v) and 5 mL of deionized water. After mixing evenly and standing for 5 min, the absorbance values were measured at 700 nm.

2.12. Storage experiments

All samples prepared freshly were stored at 4 °C, room temperature (25 °C) and 40 °C for a period of time (up to 15 days). The particle size and PDI were measured according to the section 2.3 to monitor the storage stability of all samples. The retention rate of eugenol was determined by high performance liquid chromatography

(HPLC) analysis. The retention rate was calculated by the following formula.

$$\text{Retention rate } (\%) = \frac{C_1}{C_0} \times 100 \quad (6)$$

Where C_1 represents the eugenol content of samples stored for a period of time. C_0 represents the eugenol content of samples prepared freshly before storing.

2.13. Controlled release

The controlled-release properties of eugenol in nanoparticles were studied according to a previous study (Chang, et al., 2017) with minor modifications. The simulated gastric fluid (SGF) (pH 2.0) and intestinal fluid (SIF) (pH 7.0) were mixed with equal volume of ethanol, which was used as simulated solution. The free eugenol (1.5 mg/mL) dissolved in ethanol, uncrosslinked and crosslinked nanoparticles (10 mL) were placed into dialysis bags (molecular cutoff = 7000 Da) with both ends sealed containing 10 mL of SGF, respectively. Then, all dialysis bags were placed into beakers with 150 mL of SGF and incubated for 2 h at 37 °C water bath shaker. After 2 h, 5 mL of SIF was added into dialysis bags, which was adjusted to pH 7.0. The dialysis bags were then placed into other beakers containing 150 mL of SIF and incubated for 4 h at 37 °C water bath shaker. During incubation, the release medium (2 mL) was taken out at certain intervals to measure eugenol concentration, while replenishing 2 mL of fresh release medium.

2.14. Statistical analysis

All the measurements were conducted in triplicate, and the results were presented as mean ± standard error (SD). Statistical analysis of the data was performed by the IBM SPSS 22 Statistics. The obtained mean values were subjected to Duncan's

multiple-range test. The significant level $p < 0.05$ was used in the whole study.

3. Results and discussion

3.1. Fourier transform infrared spectroscopy (FTIR) characterization

FTIR has been used to study the interaction between essential oils and wall materials (Muhoza, et al., 2019). Fig. 1A shows the FTIR spectra of NaCas, GA, eugenol and nanoparticles. For NaCas, the absorbance peak at 3299 cm^{-1} was mainly owing to the superposition of the stretching vibration of N-H and the stretching vibration of O-H. The characteristic peaks for NaCas assigned to the amide I and the amide II at 1654 cm^{-1} and 1544 cm^{-1} , which was due to the stretching of carbonyl group C=O and the symmetric stretching of N-C=O bonds, respectively (Chang, et al., 2017; Koo, Mok, Pan, & Kim, 2016). The bands at 1398 cm^{-1} and 1089 cm^{-1} referred to the carboxylate group O-C-O and weak starching of C-O, respectively (Kavousi, Fathi, & Goli, 2018). The peak at 1315 cm^{-1} assigned to the stretching vibration of amide III C-NH_2. Some researchers showed that GA was a hetero-polysaccharide of arabinogalactan and glycoproteins. For the FTIR spectra of GA, the characteristic peak of OH or NH_2 appeared at approximate 3415 cm^{-1}. The peak at about 2929 cm^{-1} was the absorbance peak of anti-symmetric stretching of CH_2 (Shaddel, et al., 2018). The peaks at 1612 cm^{-1} and 1423 cm^{-1} were due to the asymmetry and symmetric stretching vibration of COOH. The two peaks at 1228 cm^{-1} and 1074 cm^{-1} were formed by the stretching vibration of C-O.

After the complexation of NaCas and GA, the carbonyl-amide region was changed

281 significantly, the absorbance peaks of NaCas at 1315 cm^{-1} and the peaks of GA at
282 1612 cm^{-1} and 1423 cm^{-1} disappeared, indicating the electrostatic interaction between
283 the amine groups ($-NH_3^+$) of NaCas and carboxyl groups ($-COO^-$) of GA, which was
284 in accordance with previous researches (Espinosa-Andrews, Sandoval-Castilla,
285 Vázquez-Torres, Vernon-Carter, & Lobato-Calleros, 2010; Hu, Li, Zhang, Kou, &
286 Zhou, 2018). Compared with blank nanoparticles, the peaks of eugenol nanoparticles
287 at the amide Ⅰ (1627 cm^{-1}) and the amide II (1535 cm^{-1}) were red-shifted 17 cm^{-1} and
288 5 cm^{-1}, respectively, indicating that the main forces between eugenol and protein were
289 hydrogen bonding and hydrophobic interaction (Chen, Zhang, & Zhong, 2015). It
290 indicated that the eugenol was successfully encapsulated into nanoparticles.

291 Fig. 1B shows the FTIR spectra of the uncrosslinked and crosslinked eugenol
292 nanoparticles. It can be seen that TA had two large peaks at 1714 cm^{-1} and 1612 cm^{-1},
293 which was caused by the carbonyl stretching of TA (Zhan, Yang, Li, Wang, & Li,
294 2017). Both the C=O and N-H bonds was dramatically vital for infrared spectroscopic
295 analysis. The crosslinked nanoparticles only had a single peak at 1622 cm^{-1}, which
296 was attributed to the absorption peak of uncrosslinked nanoparticles at 1627 cm^{-1}
297 overlapping the TA band at 1612 cm^{-1}, and the new bands appeared at 3387 cm^{-1},
298 which indicated that TA crosslinked nanoparticles mainly through hydrogen bonding
299 interaction. Our results were in accordance with findings of Zou, et al. (2015) on the
300 utilization of the zein/TA complex particles to prepare Pickering emulsion gels.

301 ***3.2. Fluorescence spectroscopy measurements***

302 The interaction between NaCas and other molecules (eugenol and TA) can be also

303 further confirmed by fluorescence spectroscopy (Pallares, Vendrell, Aviles, &
304 Ventura, 2004). The fluorescence of NaCas was mainly due to Tryptophan (Trp)
305 residues and Tyrosine (Tyr) residues. The fluorescence absorption spectrum at the
306 excitation wavelength of 295 nm was mainly derived from Trp. Fluorescence
307 absorption spectra derived from Trp and Tyr at 280 nm excitation wavelength. Fig. 2
308 shows the intrinsic fluorescence emission spectra of NaCas at different eugenol
309 concentrations (Fig. 2A) or different TA concentrations (Fig. 2B) at 280 nm (left) or
310 295 nm (right) excitation wavelength. Fig. 2A shows that the fluorescence intensity
311 increased the increase of eugenol and the maximum emission wavelength decreased,
312 indicating the microenvironment of Trp residues and Tyr residues became more
313 hydrophobic. The changes were due to the interaction between NaCas and eugenol.
314 Our findings were similar with the previous study on the curcumin and NaCas, which
315 demonstrated that eugenol was present at the hydrophobic core of nanoparticles (Pan,
316 Zhong, & Baek, 2013).

317 Fig. 2B shows that the intrinsic fluorescence spectra of eugenol nanoparticles
318 changed in the presence of TA. The fluorescence intensity decreased significantly at
319 280 nm and 295 nm with the increase of TA concentration, demonstrating that the
320 interaction TA with protein caused the quenching of the fluorescence. Additionally,
321 the maximum emission wavelength red-shifted, indicating the addition of TA
322 enhanced the polarity of microenvironment of Trp residues and Tyr residues and
323 reduced the hydrophobicity (Chen, Zhang, & Tang, 2016). These changes may be due
324 to the conformational changes of protein caused by the addition of TA, which was

325 also confirmed by CD. These findings were consistent with the reported study (Xie, et
326 al., 2017). The modified Stern-Volmer equation (Fig. 2C) is used to identify
327 quenching type. Table 1 shows the related Stern-Volmer data, and it is well known
328 that the maximum quenching constant K_q is 2.0×10^{10} L mol^{-1} s^{-1}. It is considered as
329 static quenching when the K_q is greater than 2.0×10^{10} L mol^{-1} s^{-1}, and conversely, it is
330 dynamic quenching (Eftink, 2001). From the data obtained by Table 1, the K_q at the
331 excitation wavelengths of 280 nm and 295 nm were 1.6472×10^{11} L mol^{-1} s^{-1} and
332 1.7962×10^{11} L mol^{-1} s^{-1}, respectively. Therefore, the quenching type of NaCas caused
333 by TA was static quenching. In addition, Table 1 shows that at 280 nm and 295 nm
334 excitation wavelength, the K_b values were 1.5740×10^{6} mg/mL and 2.1582×10^{7}
335 mg/mL, respectively, and the n values were 1.4594 and 1.9327, respectively. The
336 obtained K_b values and n values showed that TA had a higher affinity with Trp than
337 Tyr, which was similar to the previous results (Chen, et al., 2018).

338 ***3.3. Circular dichroism (CD) analysis***

339 The secondary structure of protein mainly includes α-helix, β-sheet, β-turn and
340 random coil. CD is used to identify the changes of the secondary structure of protein
341 (Saxena & Wetlaufer, 1971). CD combined with fluorescence spectroscopy and FTIR
342 can be used to well understand the interaction mechanism between proteins and other
343 molecules. Therefore, the effects of TA or eugenol on the secondary structure of
344 NaCas can be established by the CD technique. Fig. 3A shows that the CD spectra of
345 protein exhibited a negative peak at 208 nm, a shoulder at 222 nm and a positive
346 absorption at 191-193 nm, which was the characteristic of α-helix (Corrêa & Ramos,

347 2009). The content of α-helix was widely estimated by the CD ellipticity at 222 nm
348 (Li, et al., 2012). β-sheet structures had a minimum of 215 nm and a positive
349 maximum at 195 nm (Corrêa, et al., 2009). Fig. 3A shows the effect of eugenol
350 concentration on the CD spectra of protein. It can be observed that the addition of
351 eugenol had no significant effect on secondary structure of the protein. The results can
352 be confirmed with the percentage of secondary structures in Table 2. The findings
353 revealed that the addition of eugenol caused the conformational change of protein in
354 accordance with the results of fluorescence spectroscopy. As is shown in Table 2 and
355 Fig. 3A, the content of α-helix (10.8～11.6%) had no significant change and β-sheet
356 exhibited irregular changes with the increasing of eugenol content. Moreover, the
357 conformational change of protein at the ratios of 1:1 and 2:1 was different from
358 others, which was similar to the change of fluorescence spectroscopy at 280 nm
359 excitation wavelength.

360 Fig. 3B shows the effect of TA concentration on the CD spectra of protein. The
361 results show that the addition of TA caused an obvious conformational change of
362 protein, which resulted from the interaction between NaCas and TA (Haslam, 1974).
363 Furthermore, the concentration of TA had a significant influence on the
364 conformational change of NaCas. At low TA concentration (0.05%), the intensity of
365 the negative peak decreased slightly, which was accordance with the previous study
366 (Zou, et al., 2015). With the increase of TA concentration, the conformational change
367 of NaCas changed obviously, indicating a significant change in protein secondary
368 structure. The results can be explained by the data from Table 2. The content of

α-helix and β-sheet increased significantly, which was helpful for enhancing the structural stabilization of NaCas (Zou, et al., 2015), and the content of β-turn and random-coil decreased obviously. In the absence of TA, the secondary structure of NaCas was composed of 11.60% α-helix, 33.80% β-sheet, 22.70% β-turn and 33.5% random-coil. The CD results also supported the previous fluorescence spectroscopy and FTIR results.

3.4. Morphological observation

TEM was used to observe the morphology of nanoparticles. Fig. 4 shows the morphology of uncrosslinked and crosslinked complex nanoparticles prepared by NaCas-GA. It can be seen that the shapes of uncrosslinked and crosslinked complex nanoparticles were both spherical with a particle size of ～140 nm. However, there existed small particles around the crosslinked nanoparticles, which may be that TA (as a cross-linker) can induce growth and aggregation of nanoparticles, because the TA concentration dramatically increased during water evaporation. The results were in agreement with a previous study reported by other research that the high concentration of TA can result in significant aggregation of nanoparticles in the formulation (Hu, Wang, Fernandez, & Luo, 2016; Zou, et al., 2015).

3.5. Thermal gravimetric analysis (TGA) analysis

TGA is used to study the thermal stability of samples and the variation of mass loss of samples as a function of temperature or time (Muhoza, et al., 2019). The DTG curves of the samples corresponding to the TGA curves are shown in Fig. 5. The TGA and DTG curves of the free eugenol showed a weight loss of 96% at 225 ^{o}C,

indicating that the free eugenol completely degraded. Figure 5 shows that the mass loss of all samples at 125 °C was mainly due to the evaporation of water. Fig. 5 shows the effect of TA concentrations on the TGA and DTG analysis curves of nanoparticles. As is shown in Fig. 5, the thermal stability of nanoparticles changed insignificantly at low concentration TA, which may indicate that the polyhydroxy group of TA did not form the covalent bond with NaCas, but interacted with NaCas by the non-covalent binding, such as the hydrogen bonds (Pérez, David-Birman, Kesselman, Levi-Tal, & Lesmes, 2014). The thermal stability of nanoparticles encapsulating eugenol was improved significantly by cross-linking using TA.

3.6. Encapsulation efficiency (EE), particle size and zeta-potential analysis

The EE, particle size and droplet size distribution of nanoparticles are shown in Fig. 6. The EE decreased with the increase of eugenol content, which might be due to the loading limitation (Woranuch, et al., 2013). Although the change of the particle size was not obvious, the turbidity of the system became bigger similar to emulsion with the increase of eugenol content. Additionally, Fig. 6 shows that the addition of TA had no obvious effect on the EE and particle size of nanoparticles. The results of zeta-potential measurement (Fig. 6) at different pH values shows that nanoparticles cross-linked by TA were stable in a wide pH range (pH 3.0-7.0) due to electrostatic repulsion. However, the uncrosslinked nanoparticles were unstable at pH 3.0 and the precipitation formed immediately. Fig. 6F shows that the precipitates existed in the bottom for the uncrosslinked nanoparticles. The results indicated that the addition of TA improved the stability of nanoparticles at the acidic condition. TA with many

galloyl residues can interact with NaCas through hydrogen bonds, which might be the main driving force (Pérez, et al., 2014). These findings were in agreement with previous studies on crosslinking of proteins using TA (Wang, et al., 2015). Zou et al (2017) also showed that adding TA can protect functional components from degradation, control their release during digestion and further improve their bioavailability.

3.7. Stability analysis of nanoparticles at different pH and heating temperatures

Fig 7 shows the effect of pH and temperature on the stability of uncrosslinked and crosslinked nanoparticles. At pH 3.0, the uncrosslinked nanoparticles precipitated while the crosslinked nanoparticles remained stable, which can be also seen from Fig. 6F. Moreover, the particle size of the uncrosslinked nanoparticles drastically increased to 250 nm, and the crosslinked nanoparticles changed insignificantly. In the range of pH 3.0-7.0, the PDI of most samples was less than 0.3, indicating that the particle size was relatively uniform. Fig. 7B, D shows that the particle size of the uncrosslinked and crosslinked nanoparticles changed insignificantly over the studied temperature range, indicating the thermal stability of the nanoparticles. Therefore, cross-linking of TA can increase the pH stability of the nanoparticles and maintain thermal stability.

3.8. Antioxidant capacity of eugenol nanoparticles

Several researches reported that eugenol exhibits high free radical scavenging ability (Chen, Shi, Neoh, & Kang, 2009). Therefore, it was important to evaluate the antioxidant activity of eugenol nanoparticles. The DPPH experiment is the most

studied method for evaluating the antioxidant efficiency of antioxidants. The results indicated that eugenol nanoparticles had higher DPPH free radical scavenging activity than free eugenol (Fig. 8A), increasing with the increase of eugenol concentration, which might be due to the hydrogen/electron transfer reactions by the abundant hydroxyl group (Dejian, Boxin, & Prior, 2005). In addition, DPPH was prepared in ethanol, which caused a certain degree of damage to the wall material and promoted the dissolution of eugenol. Similarly, the antioxidant properties of antioxidant can also be enhanced by encapsulation in other literatures (Pan, Luo, Gan, Baek, & Zhong, 2014; Wang, et al., 2016). Moreover, Fig. 8 shows that the antioxidant capacity of nanoparticles cross-linked by TA was enhanced due to synergistic antioxidant action. Apparently, the antioxidant activity of all samples increased with the increase of eugenol concentration.

Considering the presence of ethanol can damage the nanoparticles in the above experiment, the $ABTS^+$ free radical scavenging ability and the reducing power of the nanoparticles were studied (Fig. 8B and Fig. 8C). For the $ABTS^+$ free radical scavenging ability, both eugenol in uncrosslinked nanoparticles and free eugenol dissolved in ethanol were similar. However, after crosslinking, the scavenging rate of eugenol increased. Therefore, the antioxidant activity of TA can improve the antioxidant capacity of nanoparticles. However, the reducing power of eugenol in uncrosslinked and crosslinked nanoparticles was lower than free eugenol dissolved in ethanol. All in all, the antioxidant capacity of nanoparticles can be enhanced after crosslinking.

3.9. Stability of nanoparticles and slow release of eugenol in nanoparticles

The stability of uncrosslinked and crosslinked eugenol nanoparticles was further tested during storage for 15 days at 4 °C, 25 °C and 40 °C (Fig. 9). Two kinds of nanoparticles, uncrosslinked and crosslinked nanoparticles, demonstrated good stability. Slight changes in particle size and PDI were observed over time (Fig. 9). Although, with the increase of storage temperature, a small amount of precipitation of nanoparticles appeared over time. This phenomenon was because that the pH was close to the isoelectric point of NaCas (PI= 4.6), a small number of large particles aggregated and precipitated. The capability to maintain almost exactly the same particle size and PDI during the storage suggested that the coating layers, NaCas and GA, did not dissociate and the complex structure of nanoparticles was well preserved. The eugenol retention rate gradually decreased during storage, but the retention rate of eugenol in crosslinked nanoparticles was above the uncrosslinked nanoparticles, which demonstrated that TA cross-linking had a positive effect on the controlled-release of eugenol in nanoparticles. These results indicated that nanoparticles were not easily dissociated and the complex structure of nanoparticles was well preserved.

3.10. Controlled-release properties of eugenol in nanoparticles

The controlled-release properties of eugenol from nanoparticles (uncrosslinked and crosslinked nanoparticles) were studied in this paper (Fig. 11). It can be seen that the diffusion of all samples across the dialysis bags showed an upwardly convex curve. Compared with uncrosslinked and crosslinked nanoparticles, the 70% of free

479 eugenol was detected in SGF release medium and another 25% was detected in SIF
480 release medium. However, the only about 40% of eugenol in two nanoparticles was
481 released in SGF release medium and the about 22% of eugenol was detected in SIF
482 release medium. Both uncrosslinked and crosslinked nanoparticles showed no burst
483 release, indicating that they had excellent controlled-released properties. Moreover,
484 no significant difference existed between the uncrosslinked and crosslinked
485 nanoparticles. Similar results were also found in another study (Hu, et al., 2016).

486 **4. Conclusions**

487 In conclusion, the eugenol-loaded complex nanoparticles crosslinked by TA were
488 prepared successfully. The stability of nanoparticles was improved at pH 3.0 due to
489 the addition of TA. The EE was not significantly impacted by the TA content. The
490 FTIR, fluorescence spectrum and CD experiments showed that eugenol was
491 encapsulated in the hydrophobic core of the complex nanoparticles through the
492 hydrogen bond interaction and TA also interacted with NaCas by the hydrogen bond.
493 The addition of TA had significant effect on the secondary structure of NaCas. The
494 EE of TA-crosslinked nanoparticles was about 70%. Thermal gravimetric analysis
495 revealed that the degradation temperature of eugenol significantly increased from
496 77-230 °C to 200-387 °C through the nanoencapsulation. Moreover, the addition of
497 TA increased the stability of the nanoparticles at acidic conditions and played a
498 synergistic antioxidant role. During storage for 15 days under 4 °C, 25 °C and 40 °C,
499 the nanoparticles remained stable in colloid state and showed controlled-release
500 effect. Moreover, under the simulated gastrointestinal conditions, the nanoparticles

showed controlled-released properties of eugenol. This study provides valuable information on nano-delivered plant essential oils and bioactive substances by complex coacervation, as well as the use of TA in nanoparticles.

FUNDING SOURCES

The research was supported by the Natural Science Foundation of Jiangsu Province (BK20161133) and the program of "Collaborative Innovation Center of Food Safety and Quality Control in Jiangsu Province".

510 **References**

511 Chang, C., Wang, T. R., Hu, Q. B., & Luo, Y. C. (2017).
512 Caseinate-zein-polysaccharide complex nanoparticles as potential oral
513 delivery vehicles for curcumin: Effect of polysaccharide type and chemical
514 cross-linking. *Food Hydrocolloids, 72*, 254-262.

515 Chen, F., Shi, Z., Neoh, K. G., & Kang, E. T. (2009). Antioxidant and antibacterial
516 activities of eugenol and carvacrol-grafted chitosan nanoparticles.
517 *Biotechnology and Bioengineering, 104*(1), 30-39.

518 Chen, H. Q., Zhang, Y., & Zhong, Q. X. (2015). Physical and antimicrobial properties
519 of spray-dried zein–casein nanocapsules with co-encapsulated eugenol and
520 thymol. *Journal of Food Engineering, 144*, 93-102.

521 Chen, S., Zhang, N., & Tang, C. H. (2016). Influence of nanocomplexation with
522 curcumin on emulsifying properties and emulsion oxidative stability of soy
523 protein isolate at pH 3.0 and 7.0. *Food Hydrocolloids, 61*, 102-112.

524 Chen, Y., Hu, J., Yi, X. Z., Ding, B. M., Sun, W. Q., Yan, F. W., … Li, Z. S. (2018).
525 Interactions and emulsifying properties of ovalbumin with tannic acid.
526 *Lwt-Food Science and Technology, 95*, 282-288.

527 Correa, D. H. A., & Ramos, C. H. I. (2009). The use of circular dichroism
528 spectroscopy to study protein folding, form and function. *African Journal of*
529 *Biochemistry Research, 3*(5), 164-173.

530 Cortial, A., Vocanson, M., Valour, J. P., Urbaniak, S., & Briançon, S. (2014).
531 Eugenol loaded solid lipid nanoparticles: A comparative study of two

processes. *Journal of Colloid Science and Biotechnology, 3*(3), 270-278.

Eftink, M. R. Fluorescence quenching: Theory and applications. In topics in fluorescence spectroscopy; Lakowicz, J. R., Eds.; Springer US: New York, NY, 2001; 2, 53-126.

Espinosa-Andrews, H., Sandoval-Castilla, O., Vázquez-Torres, H., Vernon-Carter, E. J., & Lobato-Calleros, C. (2010). Determination of the gum arabic–chitosan interactions by fourier transform infrared spectroscopy and characterization of the microstructure and rheological features of their coacervates. *Carbohydrate Polymers, 79*(3), 541-546.

Faridi Esfanjani, A., & Jafari, S. M. (2016). Biopolymer nano-particles and natural nano-carriers for nano-encapsulation of phenolic compounds. *Colloids and Surface B Biointerfaces, 146*, 532-543.

Haslam, E., . (1974). Polyphenol-protein interactions. *Biochemical Journal, 139*(1), 285-288.

Hu, S., Wang, T., Fernandez, M. L., & Luo, Y. (2016). Development of tannic acid cross-linked hollow zein nanoparticles as potential oral delivery vehicles for curcumin. *Food Hydrocolloids, 61*, 821-831.

Hu, Y., Li, Y., Zhang, W. L., Kou, G. N., & Zhou, Z. Q. (2018). Physical stability and antioxidant activity of citrus flavonoids in arabic gum-stabilized microcapsules: Modulation of whey protein concentrate. *Food Hydrocolloids, 77*, 588-597.

Huang, D. J., Ou, B., & Prior, R. L. (2005). The chemistry behind antioxidant

554 capacity assays. *Journal of Agricultural and Food Chemistry, 53*(6),
555 1841-1856.
556 Hudson, D., & Margaritis, A. (2014). Biopolymer nanoparticle production for
557 controlled release of biopharmaceuticals. *Critical Reviews in Biotechnology,*
558 *34*(2), 161-179.
559 Joye, I. J., Davidov-Pardo, G., & McClements, D. J. (2015). Encapsulation of
560 resveratrol in biopolymer particles produced using liquid antisolvent
561 precipitation. Part 2: Stability and functionality. *Food Hydrocolloids, 49*,
562 127-134.
563 Jiang, L., Wang, W., Wen, P., Shen, M., Li, H., Ren, Y., … Xie, J. (2020). Two
564 water-soluble polysaccharides from mung bean skin: Physicochemical
565 characterization, antioxidant and antibacterial activities. *Food Hydrocolloids,*
566 *100,* 105412.
567 Kavousi, H. R., Fathi, M., & Goli, S. A. H. (2018). Novel cress seed mucilage and
568 sodium caseinate microparticles for encapsulation of curcumin: An approach
569 for controlled release. *Food and Bioproducts Processing, 110*, 126-135.
570 Koo, S. Y., Mok, I. K., Pan, C. H., & Kim, S. M. (2016). Preparation of
571 fucoxanthin-loaded nanoparticles composed of casein and chitosan with
572 improved fucoxanthin bioavailability. *Journal of Agricultural and Food*
573 *Chemistry, 64*(49), 9428-9435.
574 Kroll, J., Rawel, H. M., & Rohn, S. (2003). Reactions of plant phenolics with food
575 proteins and enzymes under special consideration of covalent bonds. *Food*

Scence and Technoogy Research, 9(3), 205-218.

Liolios, C. C., Gortzi, O., Lalas, S., Tsaknis, J., & Chinou, I. (2009). Liposomal incorporation of carvacrol and thymol isolated from the essential oil of Origanum dictamnus L. and in vitro antimicrobial activity. *Food Chemistry, 112*(1), 77-83.

Li, Y. Q., Li, J., Xia, Q. Y., Zhang, B., Wang, Q., & Huang, Q. R. (2012). Understanding the dissolution of α-zein in aqueous ethanol and acetic acid solutions. *Journal of Physical Chemistry B, 116*(39), 12057-12064.

Muhoza, B., Xia, S. Q., Cai, J. B., Zhang, X. M., Duhoranimana, E., & Su, J. K. (2019). Gelatin and pectin complex coacervates as carriers for cinnamaldehyde: Effect of pectin esterification degree on coacervate formation, and enhanced thermal stability. *Food Hydrocolloids, 87*, 712-722.

Muhoza, B., Xia, S. Q., & Zhang, X. M. (2019). Gelatin and high methyl pectin coacervates crosslinked with tannic acid: The characterization, rheological properties, and application for peppermint oil microencapsulation. *Food Hydrocolloids, 97*, 105-174.

Pérez, O. E., David-Birman, T., Kesselman, E., Levi-Tal, S., & Lesmes, U. (2014). Milk protein–vitamin interactions: Formation of beta-lactoglobulin/folic acid nano-complexes and their impacton invitro gastro-duodenal proteolysis. *Food Hydrocolloids, 38*, 40-47.

Pallares, I., Vendrell, J., Aviles, F. X., & Ventura, S. (2004). Amyloid fibril formation by a partially structured intermediate state of α-chymotrypsin. *Journal of*

Molecular Biology, 342(1), 321-331.

Pan, K., Luo, Y. C., Gan, Y. D., Baek, S. J., & Zhong, Q. (2014). pH-driven encapsulation of curcumin in self-assembled casein nanoparticles for enhanced dispersibility and bioactivity. *Soft Matter, 10*(35), 6820-6830.

Pan, K., Zhong, Q. X., & Baek, S J. (2013). Enhanced dispersibility and bioactivity of curcumin by encapsulation in casein nanocapsules. *Journal of Agricultural and Food Chemistry, 61*(25), 6036-6043.

Pereira, P. C. (2014). Milk nutritional composition and its role in human health. *Nutrition, 30*(6), 619-627.

Saxena, V. P., & Wetlaufer, D. B. (1971). A new basis for interpreting the circular dichroic spectra of proteins. *Proceedings of the National Academy of Sciences of the United States of America, 68*(5), 969-972.

Shaddel, R., Hesari, J., Azadmard-Damirchi, S., Hamishehkar, H., Fathi-Achachlouei, B., & Huang, Q. R. (2018). Use of gelatin and gum arabic for encapsulation of black raspberry anthocyanins by complex coacervation. *International Journal of Biological Macromolecules, 107*, 1800-1810.

Sharif, H. R., Goff, H. D., Majeed, H., Shamoon, M., Liu, F., Nsor-Atindana, J., … Zhong, F. (2017). Physicochemical properties of β-carotene and eugenol co-encapsulated flax seed oil powders using OSA starches as wall material. *Food Hydrocolloids, 73*, 274-283.

Shi, H., Yang, H., Zhang, X., & Yu, L. L. (2012). Identification and quantification of phytochemical composition and anti-inflammatory and radical scavenging

properties of methanolic extracts of Chinese propolis. *Journal of Agricultural and Food Chemistry, 60*(50), 12403-12410.

Sibul, F., Orcic, D., Vasic, M., Anackov, G., Nadpal, J., Savic, A., & Mimica-Dukic, N. (2016). Phenolic profile, antioxidant and anti-inflammatory potential of herb and root extracts of seven selected legumes. *Industrial Crops and Products, 83*, 641-653.

Thongkaew, C., Gibis, M., Hinrichs, J., & Weiss, J. (2014). Polyphenol interactions with whey protein isolate and whey protein isolate–pectin coacervates. *Food Hydrocolloids, 41*, 103-112.

Velmurugan, P., Singam, E. R., Jonnalagadda, R. R., & Subramanian, V. (2014). Investigation on interaction of tannic acid with type I collagen and its effect on thermal, enzymatic, and conformational stability for tissue engineering applications. *Biopolymers, 101*(5), 471-483.

Wang, Q., Li, Y., Sun, F. S., Li, X. Y., Wang, P. D., Sun, J. T., … He, G. Y. (2015). Tannins improve dough mixing properties through affecting physicochemical and structural properties of wheat gluten proteins. *Food Research International, 69*(1), 64-71.

Wang, T. R., Ma, X. Y., Lei, Y., & Luo, Y. C. (2016). Solid lipid nanoparticles coated with cross-linked polymeric double layer for oral delivery of curcumin. *Colloids and Surfaces B Biointerfaces, 148*, 1-11.

Woranuch, S., & Yoksan, R. (2013). Eugenol-loaded chitosan nanoparticles: I. Thermal stability improvement of eugenol through encapsulation.

Carbohydrate Polymers, 96(2), 578-585.

Xie, L., Wehling, R. L., Ciftci, O., & Zhang, Y. (2017). Formation of complexes between tannic acid with bovine serum albumin, egg ovalbumin and bovine beta-lactoglobulin. *Food Research International, 102*, 195-202.

Ye, A., Flanagan, J., & Singh, H. (2006). Formation of stable nanoparticles via electrostatic complexation between sodium caseinate and gum arabic. *Biopolymers, 82*(2), 121-133.

Zhan, F. C., Yang, J. C., Li, J., Wang, Y. T., & Li, B. (2017). Characteristics of the interaction mechanism between tannic acid and sodium caseinate using multispectroscopic and thermodynamics methods. *Food Hydrocolloids, 75*, 81-87.

Zhang, Y., Pan, K., & Zhong, Q. X. (2017). Eugenol nanoencapsulated by sodium caseinate: Physical, antimicrobial, and biophysical properties. *Food Biophysics, 13*(1), 37-48.

Zhang, Y. Z., Zhou, B., Liu, Y. X., Zhou, C. X., Ding, X. L., & Liu, Y. (2008). Fluorescence study on the interaction of bovine serum albumin with P-aminoazobenzene. *Journal of Fluorescence, 18*(1), 109-118.

Zou, Y., Guo, J., Yin, S. W., Wang, J. M., & Yang, X. Q. (2015). Pickering emulsion gels prepared by hydrogen-bonded zein/tannic acid complex colloidal particles. *Journal of Agricultural and Food Chemistry, 63*(33), 7405-7414.

Zhu, K., Yao, S., Zhang, Y., Liu, Q., Xu, F., Wu, G., … Tan, L. (2018). Effects of in vitro saliva, gastric and intestinal digestion on the chemical properties,

antioxidant activity of polysaccharide from Artocarpus heterophyllus Lam. (Jackfruit) Pulp. *Food Hydrocolloids, 87*, 952-959.

Zou, Y., Zhong, J. J., Pan, R. T., Wan, Z. L., Guo, J., Wang, J. M., … Yang, X. Q. (2017). Zein/tannic acid complex nanoparticles-stabilised emulsion as a novel delivery system for controlled release of curcumin. *International Journal of Food Science and Technology, 52*(5), 1221-1228.

671 **FIGURE CAPTIONS**

672 **Fig. 1.** FTIR spectra of (A) free eugenol, NaCas, GA, mixture (NaCas and GA), blank
673 nanoparticles and eugenol nanoparticles, and (B) TA, uncrosslinked nanoparticles and
674 crosslinked nanoparticles.

675 **Fig. 2.** Fluorescence emission spectra of blank nanoparticles different core wall ratios
676 (0:1, 1:4, 1:3, 1:2, 1:1 and 2:1) at excitation wavelength of 280 nm (A) and 295 nm
677 (B), crosslinked nanoparticles using TA (the content of TA 0.05%, 0.1%, 0.2% and
678 0.4%) at excitation wavelength of 280 nm (C) and 295 nm (D) and linear plot of F0/F
679 versus [TA] for the determination of the quenching type (E) and $\log_{10}$[(F0-F)/F]
680 versus $\log_{10}$[TA] for the determination of the binding constant of TA with NaCas (F).

681 **Fig. 3.** Far-UV CD spectra of the effects of (A) the different eugenol / NaCas mass
682 ratios (0:1, 1:4, 1:3, 1:2, 1:1 and 2:1, w/w) and (B) TA concentrations (0, 0.05%,
683 0.1%, 0.2%, 0.3% and 0.4%, w/v) on the secondary structure of NaCas.

684 **Fig. 4.** TEM images of uncrosslinked (A, B) and crosslinked (C, D) nanoparticles.

685 **Fig. 5.** TGA and DTG thermo grams of free eugenol (A) and crosslinked
686 nanoparticles using TA (the TA content 0.05% (B), 0.1% (C), 0.2% (D) and 0.3%
687 (E)).

688 **Fig. 6.** Effect of EE, particle size and particle size distribution of different wall ratios
689 (1:4, 1:3, 1:2, 1:1 and 2:1) (A, C) and TA concentrations (0.05%, 0.1%, 0.2%, 0.3%
690 and 0.4%) (B, D) on nanoparticles. (E) zeta-potential of control (without eugenol),
691 uncrosslinked nanoparticles (without TA), crosslinked nanoparticles (TA contents of
692 0.05%, 0.1% and 0.2%). (F) Visible picture of 0.05% TA crosslinked nanoparticles

693 (a1, a2) and uncrosslinked nanoparticles (b1, b2) at pH 3.0 and pH 4.0.

694 **Fig. 7.** Stability of uncrosslinked and crosslinked nanoparticles at different pH (A, B.

695 3.0, 4.0, 5.0, 6.0 and 7.0) and temperatures (C, D. 60, 80, 90 and 100 ^{o}C).

696 **Fig. 8.** Antioxidant capacity of free eugenol, uncrosslinked nanoparticles and

697 crosslinked nanoparticles (A, DPPH free radicals scavenging ability; B, $ABTS^{+}$ free

698 radicals scavenging ability; and C, Total reducing power).

699 **Fig. 9.** Storage stability (particle size and PDI) of uncrosslinked nanoparticles (A, B)

700 and crosslinked nanoparticles (C, D).

701 **Fig. 10.** Retention rate of eugenol in uncrosslinked nanoparticles (A) and crosslinked

702 nanoparticles (B).

703 **Fig. 11.** Evaluation of eugenol-loaded complex nanoparticles for kinetic release

704 profile under simulated gastrointestinal fluids.

705 Table 1. Correlation fluorescence quenching data parameters of NaCas interaction

706 with TA.

Wavelength(nm)	Kq	Ksv	Quenching type	K_b	n
280	1.6472×10^{11}	1.6472×10^{3}	Static quenching	1.5740×10^{6}	1.4594
295	1.7962×10^{11}	1.7962×10^{3}	Static quenching	2.1582×10^{7}	1.9327

707

Table 2. Secondary structure fractions of nanoparticles at different eugenol/NaCas ratios or TA concentrations.

	α-helix (%)	β-sheet（%）	β-turn（%）	random-coil（%）
Eugenol/NaCas ratios				
0:1	11.30±0.32^{a}	42.70±0.32^{d}	20.90±0.25^{bc}	29.90±0.32^{b}
1:4	11.30±0.24^{a}	37.90±0.73^{b}	21.90±0.33^{d}	32.00±0.40^{c}
1:3	11.40±0.47^{a}	39.70±0.39^{c}	21.60±0.37^{cd}	31.00±0.52^{bc}
1:2	11.60±0.43^{a}	33.80±0.67^{a}	22.70±0.46^{e}	33.50±0.32^{d}
1:1	10.80±0.70^{a}	43.00±0.25^{d}	20.60±0.37^{b}	30.40±0.41^{b}
2:1	11.50±0.25^{a}	49.70±0.18^{e}	19.10±0.24^{a}	27.40±1.03^{a}
TA concentrations				
0	11.60±0.32^{a}	33.80±0.24^{a}	22.70±0.25^{d}	33.50±0.23^{e}
0.05%	12.70±0.47^{a}	49.00±0.78^{c}	18.60±0.30^{c}	26.60±0.98^{d}
0.1%	15.40±0.41^{b}	45.00±1.10^{b}	18.10±0.41^{c}	25.60±0.23^{c}
0.2%	17.50±0.48^{c}	63.90±1.68^{e}	14.50±0.54^{b}	17.60±0.27^{b}
0.3%	18.60±1.03^{d}	61.30±0.70^{d}	14.10±0.60^{b}	16.60±0.19^{b}
0.4%	31.20±0.27^{e}	65.20±0.58^{e}	12.20±0.52^{a}	15.10±0.27^{a}

Mean values ± standard deviation (n = 3). Different subscript letters in the same column indicate significantly different ($P < 0.05$).

713 **Fig.1**

714

715

716

717

718

719

720

721

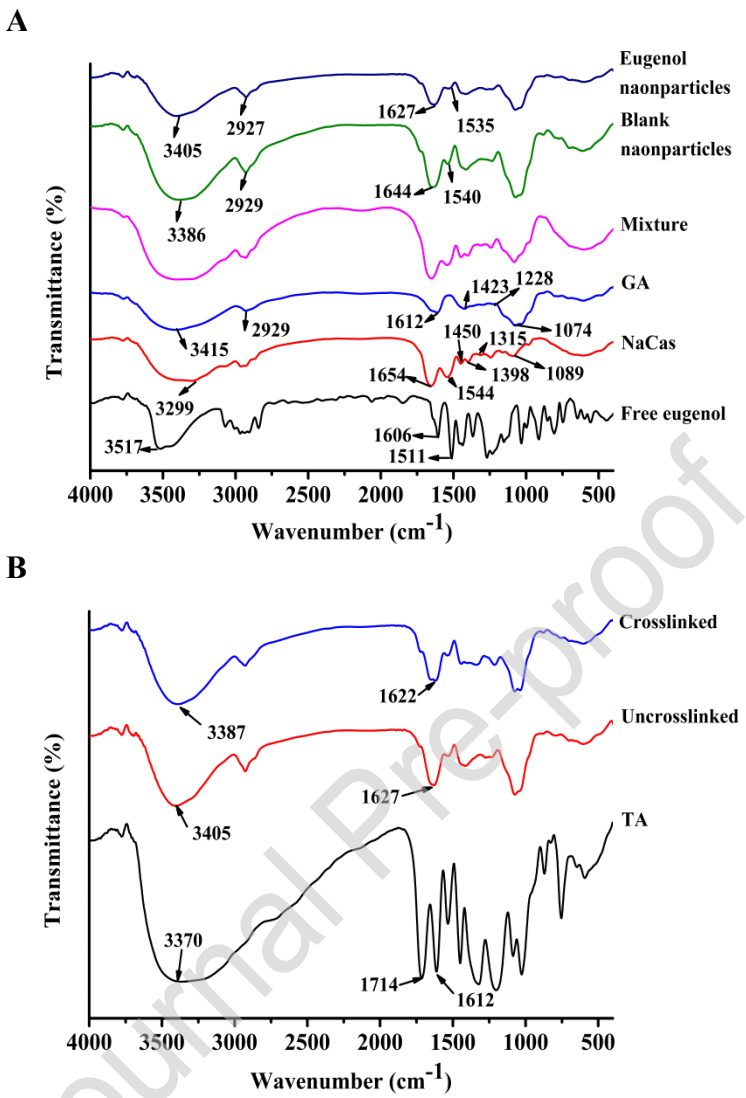

Fig. 2

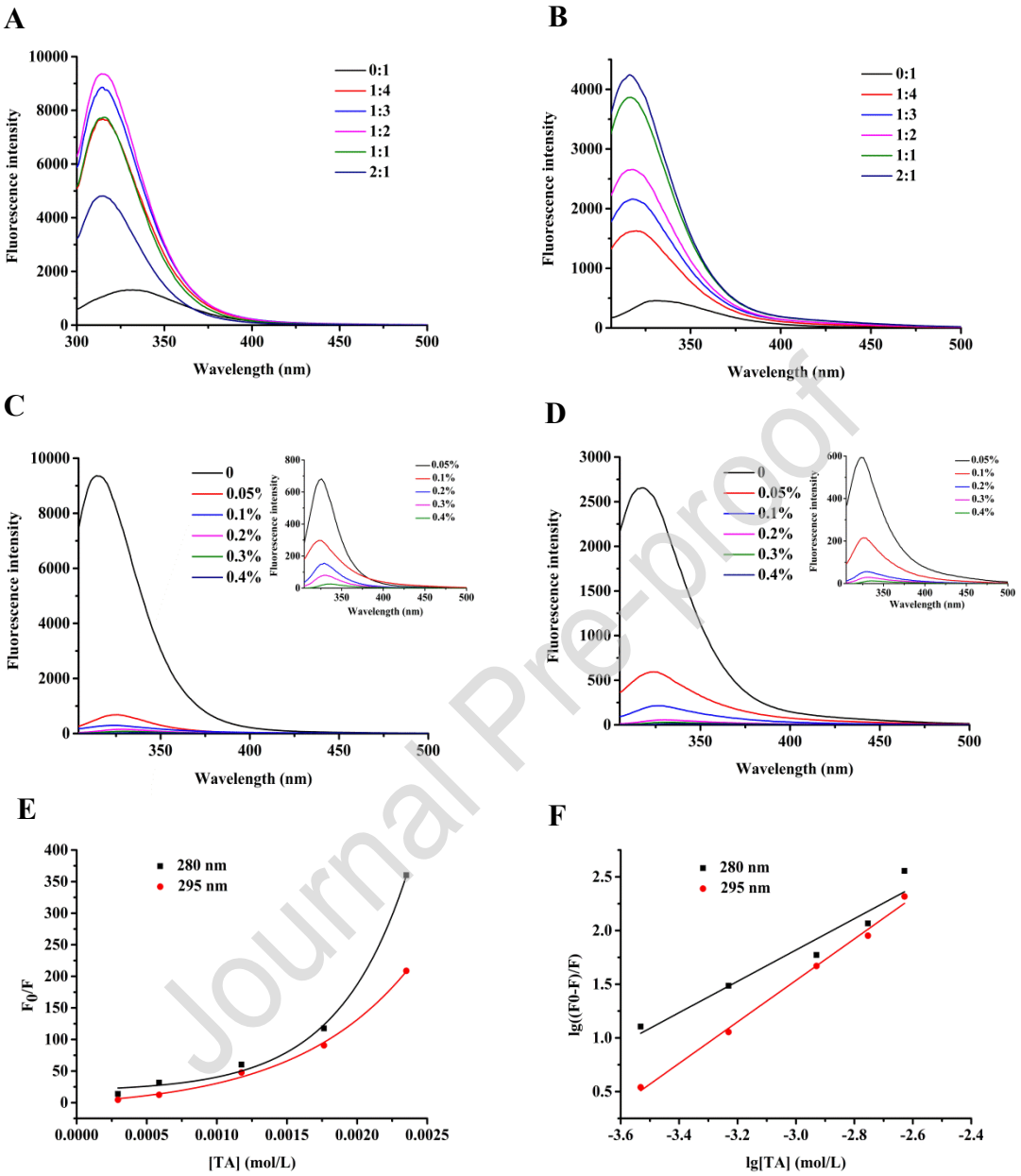

Fig. 3

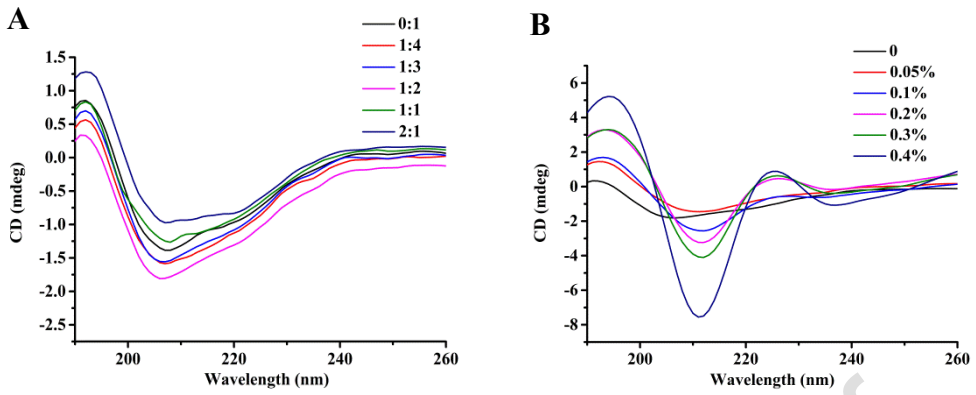

Fig. 4

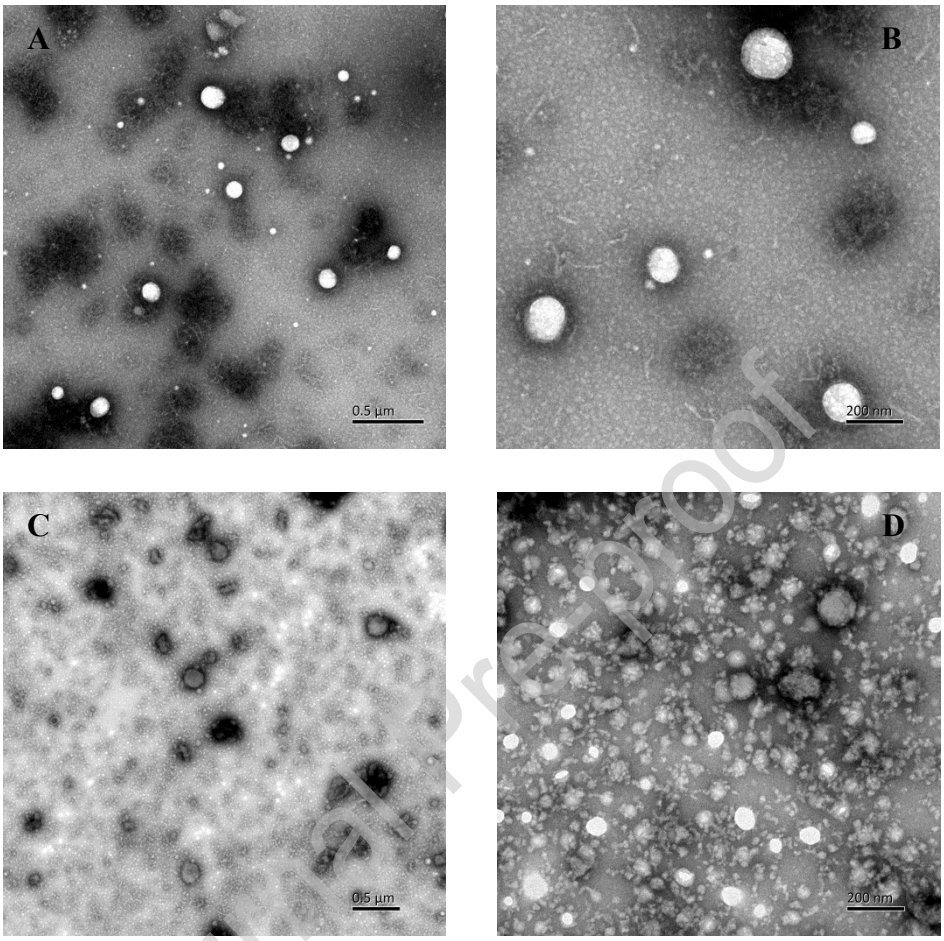

781 **Fig. 5**

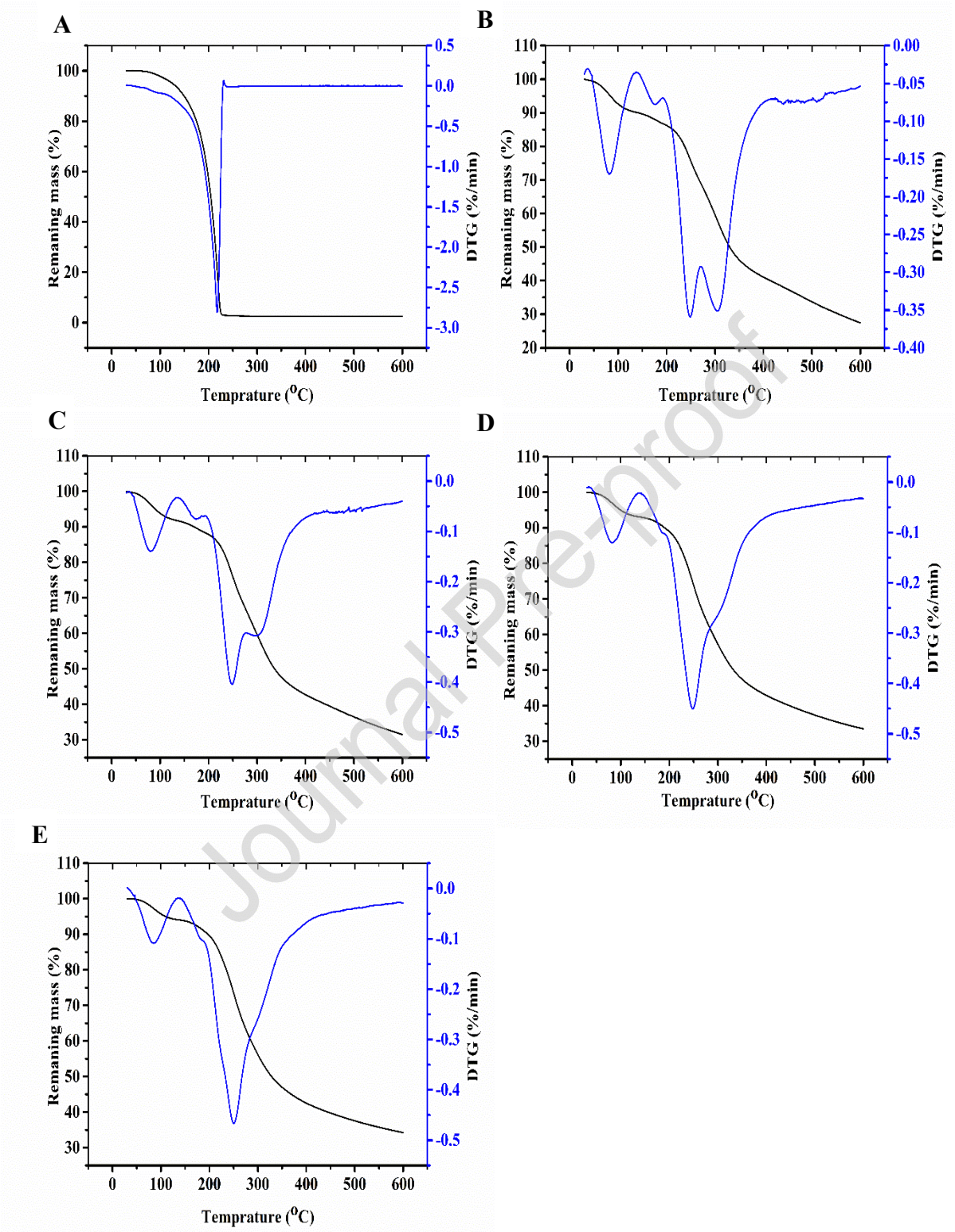

Fig. 6

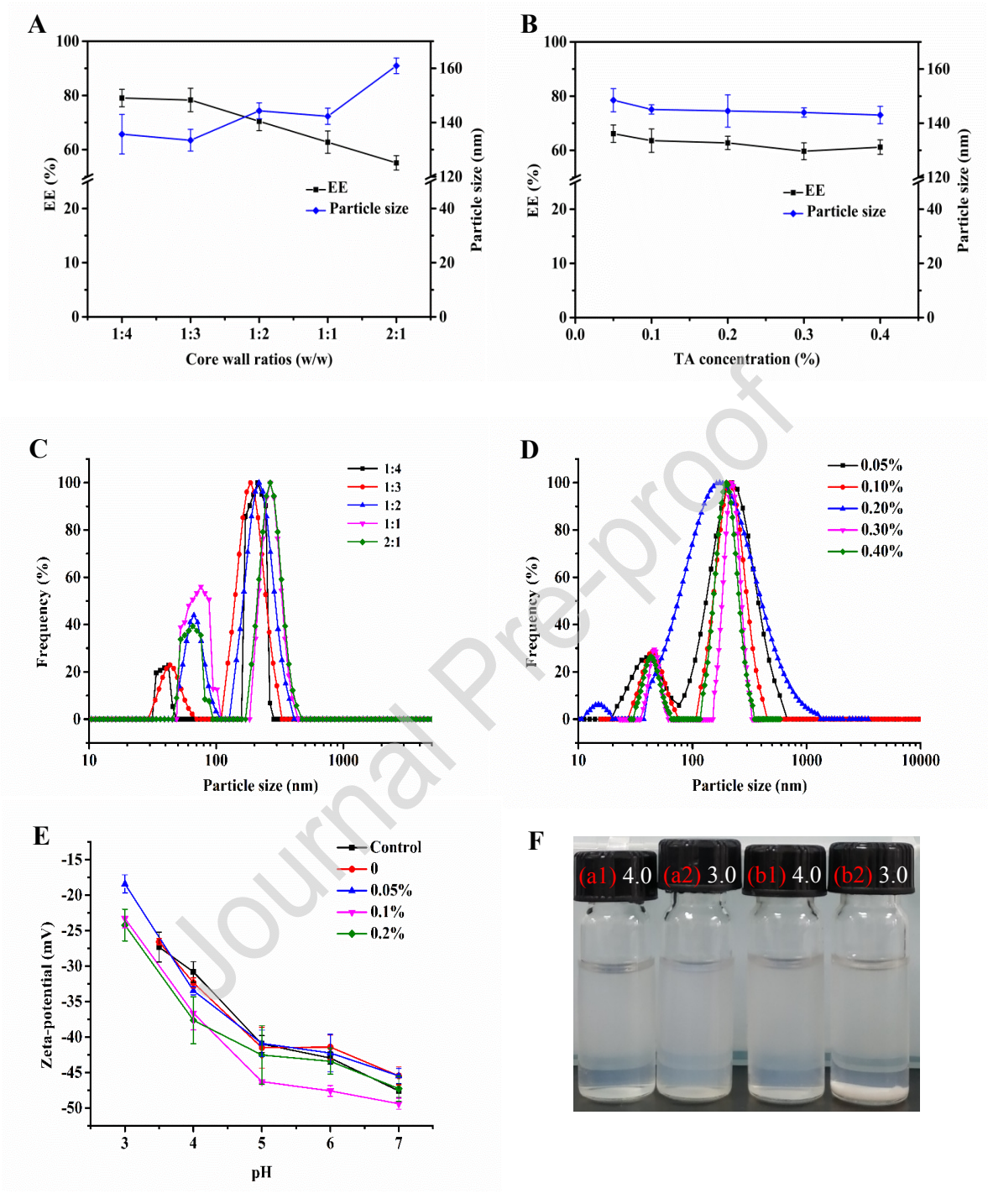

Fig. 7

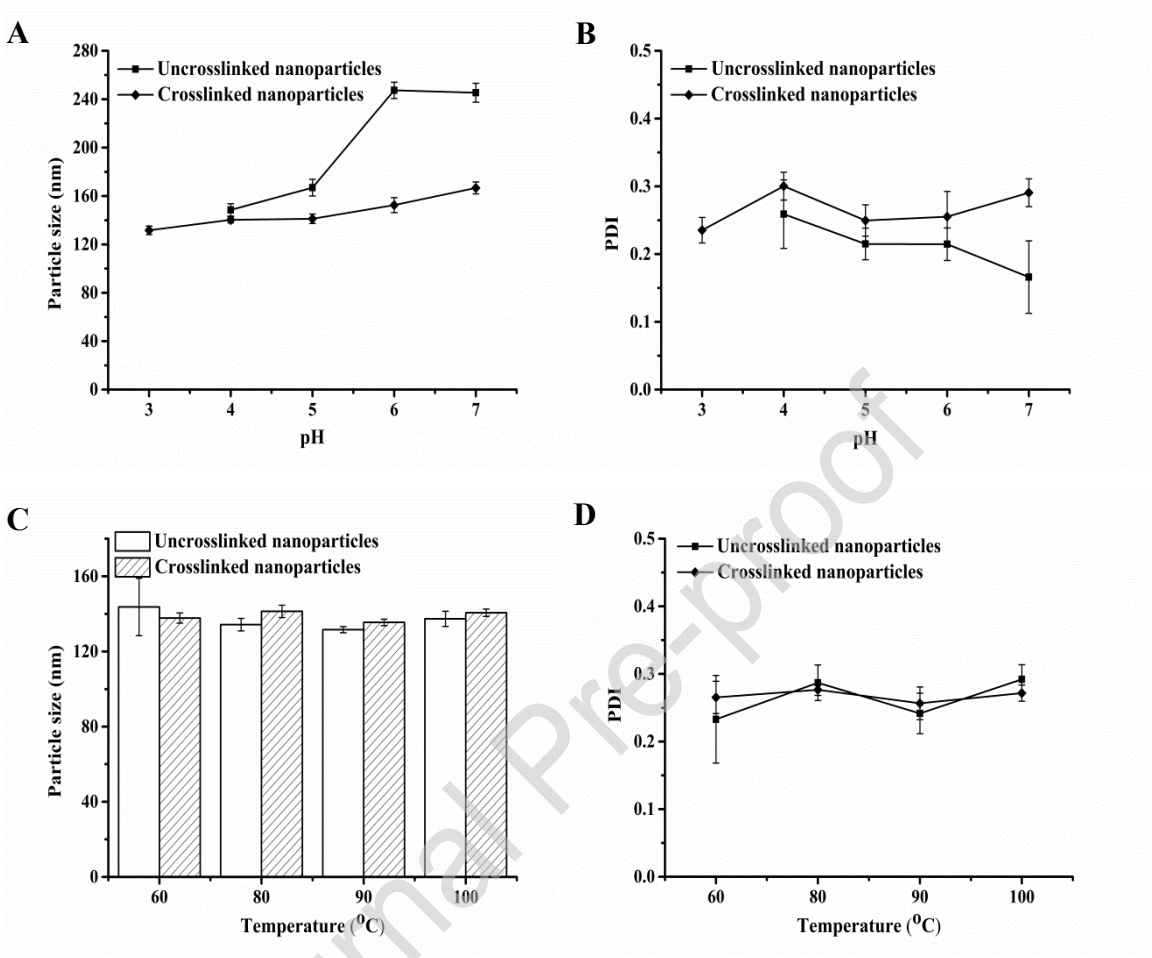

825 **Fig. 8**

826
827
828
829
830
831
832
833
834
835
836

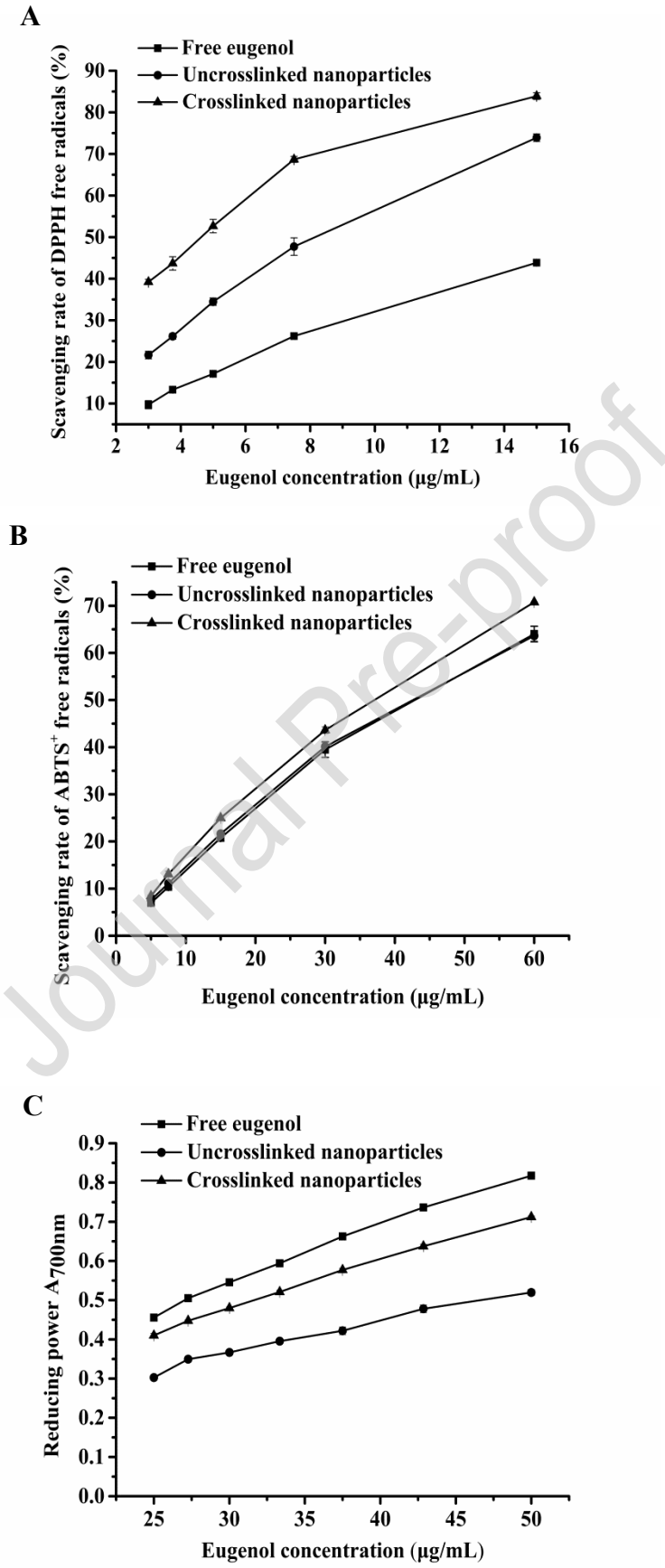

Fig. 9

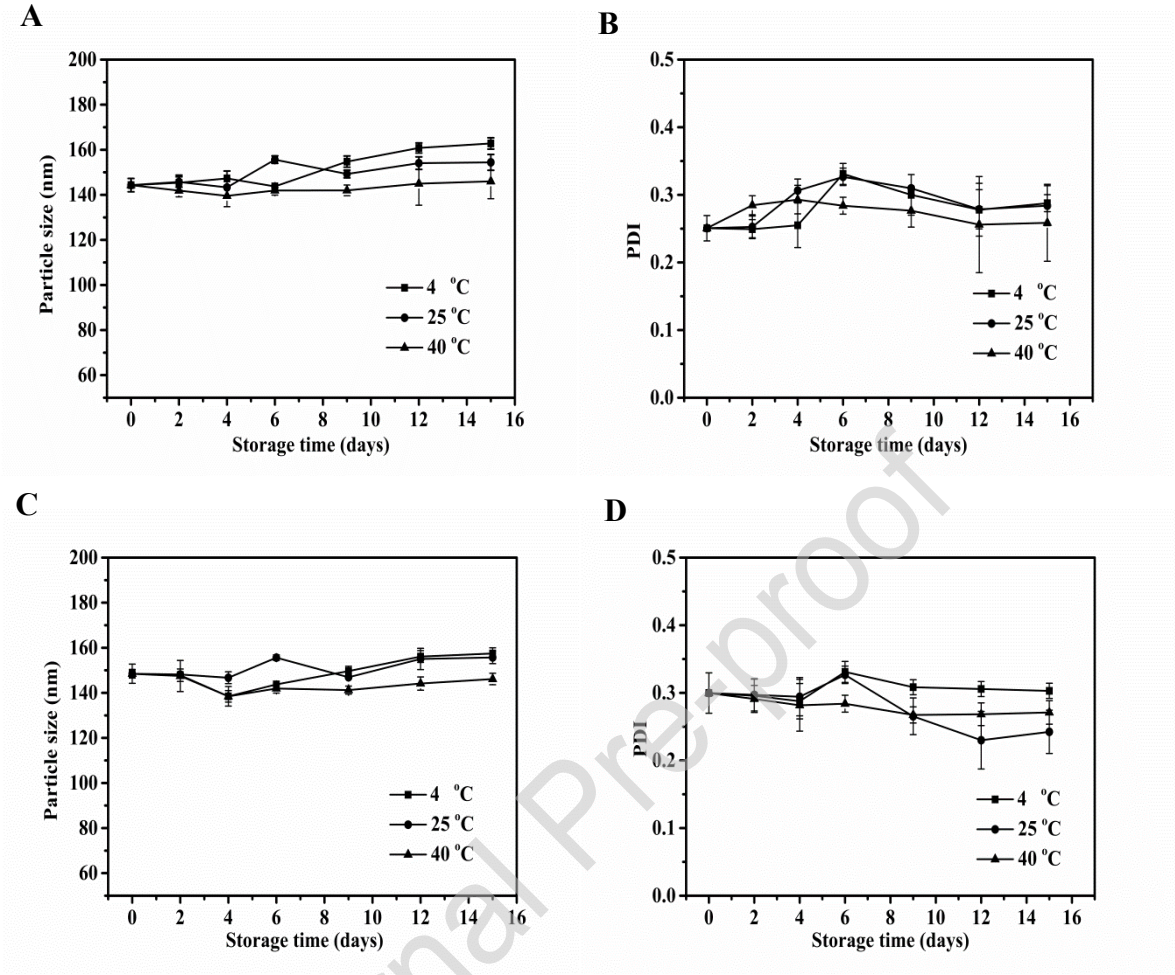

Fig. 10

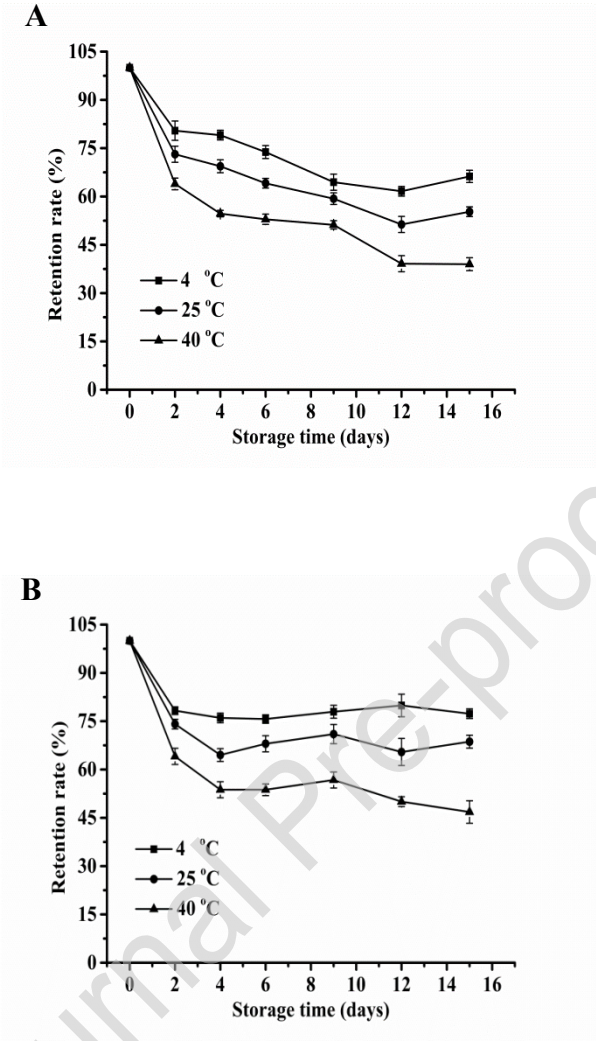

Fig. 11

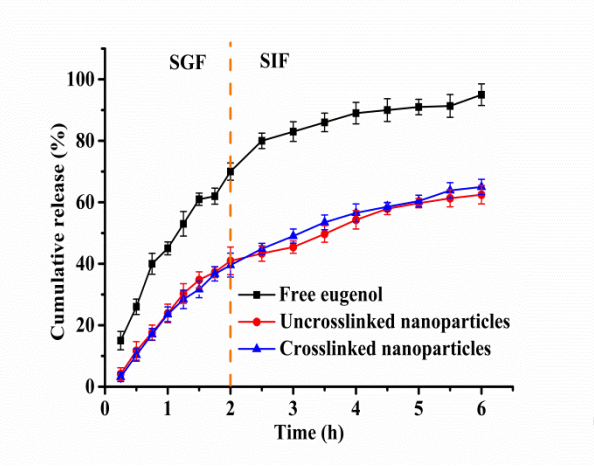

Conflict of Interest

The authors declare no conflict of interest.

Author Statement

Dandan Cao: Conceptualization and Methodology; Investigation; Writing - Original Draft; Visualization.

Chengsheng Jia: Conceptualization and Methodology; Supervision.

Suping Ji: Writing - Review & Editing.

Xiaoming Zhang: Resources.

Bertrand Muhoza: Writing - Review & Editing.

Highlights

- The biopolymer nanoparticles cross-linked by tannic acid were prepared.
- The biopolymer nanoparticles cross-linked by tannic acid had small particle size (about 150 nm) and encapsulation efficiency (about 70%)
- Tannic acid cross-linked nanoparticles showed better stability to acid environment.
- The cross-linked nanoparticles had the possibility of nano-delivering plant essential oils.